Journal of The Electrochemical Society, **146** (11) 3963-3969 (1999)
S0013-4651(99)02-078-9 CCC: $7.00 © The Electrochemical Society, Inc.

Irreversible Capacities of Graphite in Low-Temperature Electrolytes for Lithium-Ion Batteries

M. C. Smart,[a,*] B. V. Ratnakumar,[a,,z] S. Surampudi,[a,**] Y. Wang,[b] X. Zhang,[b] S. G. Greenbaum,[b,**] A. Hightower,[c,*] C. C. Ahn,[c] and B. Fultz[c,**]**

[a]*Jet Propulsion Laboratory, California Institute of Technology, Pasadena, California 91109, USA*
[b]*Department of Physics, Hunter College of City University of New York, New York, New York 10021, USA*
[c]*Division of Engineering and Applied Science, California Institute of Technology, Pasadena, California 91125, USA*

Carbonaceous anode materials in lithium-ion rechargeable cells exhibit irreversible capacity, mainly due to reaction of lithium during the formation of passive surface films. The stability and kinetics of lithium intercalation into the carbon anodes are determined by these films. The nature, thickness, and morphology of these films are in turn affected by the electrolyte components, primarily the solvent constituents. In this work, the films formed on graphite anodes in low-temperature electrolytes, *i.e.*, solutions with different mixtures of alkyl carbonates and low-viscosity solvent additives, are examined using electrochemical impedance spectroscopy (EIS) and solid-state ^{7}Li nuclear magnetic resonance techniques. In addition, other *ex situ* studies such as X-ray diffraction, transmission electron microscopy, and electron energy loss spectroscopy were carried out on the graphite anodes to understand their microstructures.

Manuscript submitted February 19, 1999; revised manuscript received June 2, 1999.

Nonaqueous electrolyte solutions in current lithium-ion cells achieve stability toward the graphite anode (negative electrode) via the formation of passive surface films on the anode surface. These films are composed of reaction products resulting from electrolyte reduction and some reduced lithium. These films reportedly contain various lithium compounds, such as lithium carbonate (Li_2CO_3), lithium oxide (Li_2O), lithium hydroxide (LiOH), lithium alkoxides, lithium fluoride (LiF), as well as electrolyte salt reduction products that are still to be accurately characterized.[1] Relative amounts of these constituents are also equally uncertain. In addition to the expense of lithium for such surface films, termed solid electrolyte interphase (SEI),[2] a portion of lithium might be "trapped" in the anode material and is "kinetically inaccessible." Consequently, a differential exists between the intercalated lithium (charge capacity) and deintercalated lithium (discharge capacity), which is loosely termed irreversible capacity. This irreversible capacity depends not only on the rate of lithiation during the formation cycles and the temperature, but also on the extent of charge-discharge cycling, during which the surface film may grow. Irreversible capacity is typically estimated as the cumulative differential in the capacity after five cycles (one cycle in some reports), when the charge capacity/discharge capacity ratio approaches unity.

It is difficult to separate the irreversible capacity into a component involving SEI formation and a component involving capacity loss due to kinetic effects, unless one of the components is estimated by a nonelectrochemical method. In this work, we attempted such a study on SEI formation on graphite in different electrolyte solutions using solid-state ^{7}Li nuclear magnetic resonance (NMR). Solid-state ^{7}Li NMR has been commonly used for qualitative detection and characterization of lithium intercalation in (and the SEI formation on) graphite and disordered carbons.[3-8] However, this technique has not been used extensively for quantitative determinations. In this work, the surface films were also examined *ex situ* by transmission electron microscopy (TEM) for elucidating the microstructure of film-covered graphite electrodes. These studies were further complemented by electrochemical impedance spectroscopy (EIS) measurements to understand the surface film characteristics of graphite anodes in different electrolytes.

Improving low-temperature performance of lithium-ion cells remains a formidable technical challenge. The present investigation is an outgrowth of our previous studies[9] of novel electrolyte formulations for low-temperature performance. Similar efforts to improve the properties of electrolytes at low temperatures are being made elsewhere.[10-14] Our recent results have shown that a ternary mixture of alkyl carbonates, *i.e.*, 1:1:1 (vol. %) of EC (ethylene carbonate):DEC (diethyl carbonate):DMC (dimethyl carbonate) with 1 M $LiPF_6$ exhibits favorable electrochemical characteristics and performs rather well at −20°C compared to typical binary mixtures.[15] To further enhance the performance at low temperatures, we are examining the effects of adding various cosolvents, with reduced viscosity and lower freezing points, to the ternary solvent mixtures. Such solvent additives examined here include aliphatic esters, *i.e.*, specifically methyl acetate (MA) and ethyl acetate (EA), and aliphatic ethers, such as 1,2-dimethoxyethane (DME), some of which have been characterized and reported earlier.[16,17] In addition, electrolyte solutions based on two conventional binary solvent mixtures with 30 vol % EC and 70 vol % DMC and DEC have also been studied for comparison.

Using the combination of film resistance values from ac impedance and ^{7}Li NMR peak intensities for nonintercalated lithium and the irreversible capacities from electrochemical measurements, we have been able to obtain a quantitative agreement between the SEI formation and irreversible capacities. With the TEM and X-ray diffraction (XRD) measurements on the cycled electrode, some chemical and microstructural heterogeneities have been identified.

Experimental

The effects of different electrolytes on the surface film characteristics and irreversible capacity of graphite (KS44) were determined in three-electrode, O-ring-sealed glass cells containing spiral rolls of graphite, lithium counter electrodes, and lithium reference electrodes separated by two layers of porous polypropylene (Celgard 2500). The graphite anodes used for these studies were fabricated with 6 wt % polyvinylidene difluoride (PVDF) binder, without any conductive diluent. The carbonate-based solvents (EC, DMC, and DEC), containing $LiPF_6$ salt in the desired concentration, were purchased from Mitsubishi Chemicals (battery grade) with less than 50 ppm water. The ester solvents (MA and EA) were purchased from Aldrich and stored over Li metal chips and molecular sieves prior to use. Electrochemical measurements were made using an EG&G Princeton Applied Research potentiostat/galvanostat interfaced with an IBM PC, using Softcorr 352. A Solartron 1255 frequency response analyzer was used with this potentiostat for impedance measurements, with M388 software. Charge-discharge measurements and cycling were performed with an Arbin battery cycler. The cycling

* Electrochemical Society Student Member.
** Electrochemical Society Active Member.
z E-mail: Ratnakumar.v.Bugga@JPL.NASA.gov

S0013-4651(99)02-078-9 CCC: $7.00 © The Electrochemical Society, Inc.

tests were carried out at 0.25 and 0.5 mA/cm^2 for Li intercalation and deintercalation to the cutoff potentials of 0.025 and 1.0 V *vs*. Li, respectively, with a 15 min interval between the charge/discharge steps. For the lithiation process, a constant-potential (0.025 V *vs*. Li) step for 3 h was added subsequent to the constant-current lithiation.

Before the analytical measurements, including ^{7}Li NMR and TEM, the electrodes typically underwent about 40 charge-discharge cycles as part of performance characterization at various rates and temperatures. The graphite electrodes were washed repeatedly in DMC and dried in an argon-filled glove box. The powdered electrode materials were packed into tightly sealed 7.5 mm zirconia NMR rotors. About 300 mg of each sample was utilized for the NMR measurements, which were conducted on a Chemagnetics CMX-300 spectrometer operating at a ^{7}Li resonance frequency of 117 MHz. Aqueous LiCl was employed as a chemical shift reference. Both static and magic angle spinning (MAS) NMR spectra were obtained at 23°C, the latter using spin rates of about 5 kHz. To facilitate quantitative determination of Li-containing species, the spin axis was deliberately offset from the magic angle by about 1°, thus decreasing the intensity of the spinning side bands.

X-ray diffractometry was performed on cycled graphite with an INEL CPS-120 powder diffractometer using Mo Kα radiation (λ = 0.7092 Å). The anode materials were sealed in Pyrex capillary tubes under Ar using paraffin wax. The fractions of LiC_6 and LiC_{12} phases were determined by comparing the intensities of the LiC_6 (003) and LiC_{12} (005) peaks, which are well separated in 2θ angle. Detection limits were determined primarily by the statistical quality of the data and estimated to be about 3%.

TEM was performed with Philips EM 430 and Philips EM 420 instruments. Samples were mixed with Flourinert™ and crushed with a mortar and pestle in an argon-filled glove box. The powdered mixture of anode material was placed on a holey carbon microscope grid. Electron energy loss spectroscopy (EELS) was performed on the TEM samples using a Gatan 666 parallel detection magnetic prism spectrometer attached to a Philips EM420 transmission electron microscope. The energy resolution of the spectrometer was approximately 1.2 eV with a dispersion of 0.2 eV per channel. Measurements were performed using 100 keV electrons with a spectrometer collection angle of 50 mrad. EELS measurements were made difficult by the tendency of Li to undergo "knock-on damage" under 100 keV electron-beam. This was overcome by maintaining a relatively diffuse beam.

Results and Discussion

Various electrochemical methods were used to determine the kinetics of lithium intercalation and deintercalation and charge-discharge characteristics at different temperatures. The results relative to the SEI characteristics and reversible and irreversible capacities are presented in the following sections.

Reversible and irreversible capacities.—The electrolytes selected for these studies are expected to differ considerably in their stability toward graphite, their observed irreversible capacities, their SEI formation, and perhaps in their cointercalation characteristics. The electrolyte formulations investigated in this study contained the following solvent mixtures (expressed in vol %)

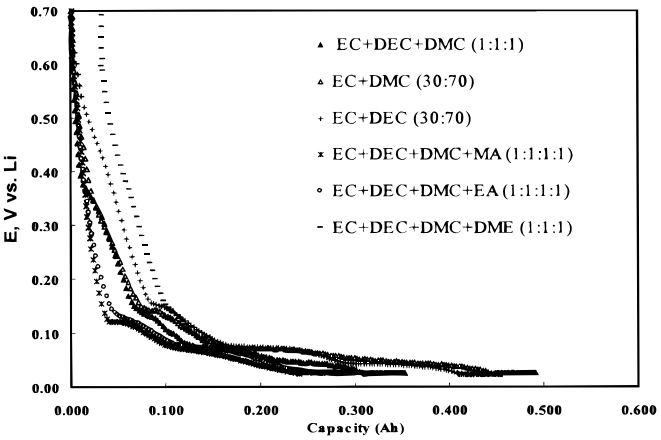

Figure 1. First intercalation process of lithium into graphite in different electrolytes containing 0.75 M $LiPF_6$ and different solvent mixtures, *i.e.*, EC + DEC + DMC, EC + DMC, EC + DEC, EC + DEC + DMC + MA, EC + DEC + DMC + EA, and EC + DMC + DEC + DME.

1. EC + DEC + DMC (1:1:1)
2. EC + DEC (30:70)
3. EC + DMC (30:70)
4. EC + DEC + DMC + MA (1:1:1:1)
5. EC + DEC + DMC + EA (1:1:1:1)
6. EC + DEC + DMC + DME (1:1:1:1)

The salt ($LiPF_6$) concentration in all these solutions was 0.75 M. The profiles of lithium intercalation into graphite in the six electrolytes under study are shown in Fig. 1.

Typically, lithium reduced at potentials ≥200 mV *vs*. Li is utilized in the formation of the surface film on the graphite anode and, thus, is not realizable in the subsequent delithiation. In general, electrolytes based on the binary and ternary solvent mixtures of alkyl carbonates containing DMC facilitate rapid film formation compared to DEC-based electrolyte, as evidenced by a sharper fall in the potential during the first lithiation. Accordingly, the irreversible capacities in these solutions are expected to be lower. In the solutions based on the ester additives, the electrode potential drops more sharply to ~120 mV during the first lithiation, suggesting that a protective surface film is formed more readily, without expending much lithium. In contrast, in the DME-based solution, considerable lithium is consumed before the electrode potentials approach lithium-intercalation values. Accordingly, the corresponding irreversible capacity is expected to be larger. These results indicate that the facility of forming the SEI decreases (and the expected irreversible capacity increases) in the following trend: EC-DEC-DMC-MA > EC-DEC-DMC-EA > EC-DMC > EC-DEC-DMC ≥ EC-DMC > EC-DEC > EC-DEC-DMC-DME.

The reversible and irreversible capacities of graphite in these electrolytes are listed in Table I. The reversible capacities represent

Table I. Reversible and irreversible capacities of graphite in different electrolytes.

Solvent	Reversible capacity First cycle	Irreversible capacity First cycle	Reversible capacity Fifth cycle	Irreversible capacity Fifth cycle	NMR intensity of nonintercalated (as % of total Li)
EC-DMC-DEC	227	106	240	127	22 ± 2
EC-DMC	302	95	313	123	25 ± 2
EC-DEC	268	107	275	137	24 ± 2
EC-DMC-DEC-MA	201	37	236	57	25 ± 2
EC-DMC-DEC-EA	210	50	214	68	35 ± 3
EC-DMC-DEC-DME	147	138	188	192	54 ± 4

S0013-4651(99)02-078-9 CCC: $7.00 © The Electrochemical Society, Inc.

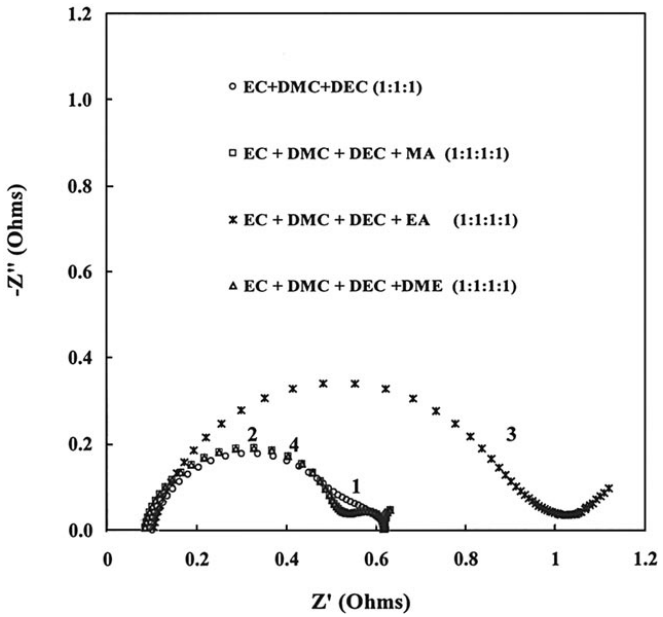

Figure 2. Nyquist plots of graphite anode in electrolytes containing 0.75 M $LiPF_6$ and different solvent mixtures, *i.e.,* (1) EC + DEC + DMC, (2) EC + DEC + DMC + MA, (3) EC + DEC + DMC + EA, and (4) EC + DMC + DEC + DME after (five) formation cycles.

the capacities delivered in the fifth deintercalation step, whereas the irreversible capacities were cumulative during these formation cycles. The capacities in Table I show that electrolytes containing quaternary aliphatic ester additives, such as methyl acetate and ethyl acetate, result in low irreversible capacities, implying that protective surface films are readily formed on the electrode surface in these electrolytes. The exclusively carbonate-based electrolytes displayed similar behavior, with higher DMC content resulting in more protective surface films. In contrast, the electrolyte with DME cosolvent showed the highest irreversible capacity and lowest reversible capacity, suggesting that the solvent is more reactive with the lithiated carbon and/or the electrolyte salt and forms less protective surface films. Overall, the reversible capacities obtained for the lithium-graphite cells studied (Table I) are marginally lower than expected due to a high cutoff potential (0.025 V *vs.* Li/Li^+) for intercalation.

Despite their low irreversible capacities, the ester additives exhibit low reversible capacities, especially after charge-discharge cycling. This was determined from charge/discharge cycling and was further confirmed from electrochemical polarization techniques (which will be reported in the future) to be due to the high resistance exhibited by the surface films to charge transfer (lithium intercalation/deintercalation) in the ester-based solutions.

AC impedance.—To characterize the surface films on graphite electrodes in these electrolyte solutions with different solvent mixtures, EIS measurements were performed both initially (*i.e*., after five formation cycles) and again after detailed electrochemical tests (*i.e.*, about 40 charge-discharge cycles) to understand the rate capability and kinetics of Li intercalation at different temperatures. The ac impedance data were obtained in the frequency range 100 kHz to 5 mHz at low ac amplitude of <5 mV. The impedance plots of graphite electrodes in the electrolytes containing the ternary and quaternary solvent mixtures are shown in the Nyquist or Cole-Cole form in Fig. 2.

As may be seen qualitatively in the figures, the impedance patterns in the DME-based and MA-based electrolytes are similar in shape as well as values and are only marginally higher than that of the ternary system. In the EA-based solution, on the other hand, the impedance is considerably larger. These data have been analyzed using an equivalent circuit[18] consisting of a series (electrolyte/electrode) resistance and two parallel resistance-capacitance (RC) circuits (the latter with a parallel Warburg impedance) to represent the surface film charging and interfacial charge-transfer processes, respectively. The parameters in the equivalent circuit were calculated by a nonlinear least-squares fit (Table II) using the Boukamp method.[19] The series resistance is the highest in the ternary system, consistent with the ionic conductivity measurements; the quaternary solvent expectedly improves the ionic conductivity. The series resistance increases as EC-DEC-DMC-MA ≤ EC-DEC-DMC-DME < EC-DEC-DMC-EA < EC-DEC-DMC ≤ EC-DMC < EC-DEC. The film resistance, obtained from the first relaxation loop, is the highest for EC-DEC-DMC-MA and decreases as EC-DMC-DEC-MA > EC-DEC-DMC-DME > EC-DEC-DMC > EC-DMC > EC-DEC-DMC-EA > EC-DEC (Table II). The resistances of the surface films in the DME-based and MA-based solutions are fairly close, although the irreversible capacities are noticeably different. It is reasonable to conclude that the larger the irreversible capacity, the larger the film thickness, since more lithium is consumed in the SEI formation. A combination of high irreversible capacity and low film resistance for the DME-based solution (relative to the ternary system) would therefore suggest that relatively thicker surface film is formed in this electrolyte. Furthermore, this surface film appears to be insufficiently protective, as evident from a continued decay of the reversible capacity upon cycling, and could be viewed as porous (nonbarrier type). In the MA-based solution, on the other hand, the SEI is possibly thinner, barrier-type and more resistive. The higher resistivity of the SEI in ester-based solutions is also evident in the slower kinetics of lithium intercalation-deintercalation, especially after cycling. This is further illustrated in the ac impedance data after additional charge-discharge cycling (for about 40 cycles) (Fig. 3). The series resistance in the cells with ester additives increases appreciably and the performance falls sharply, whereas that in the ternary system remains unchanged. This may be attributed to the continued reaction of the ester additives despite a more resistive SEI. This increase is more pronounced with the MA additive compared to the EA additive. In the DME-based electrolyte, on the other hand, the impedance decreases slightly after charge-discharge cycling, consistent with a porous surface film formed in this electrolyte. The charge-transfer resistance obtained from the low-frequency relaxation loop

Table II. Interfacial properties of graphite anodes in different electrolytes, obtained from ac impedance.

	Series (Electrolyte) resistance (Ω cm^2)		Film resistance (Ω cm^2)		Charge-transfer resistance (Ω cm^2)	
Solvent	After formation	After cycling	After formation	After cycling	After formation	After cycling
EC-DMC-DEC	14	18	22	9	47	20
EC-DMC	14	21	20	17	22	25
EC-DEC	15	18	9	25	24	10
EC-DMC-DEC-MA	12	387	58	47	13	465
EC-DMC-DEC-EA	14	207	19	54	104	460
EC-DMC-DEC-DME	12	16	56	10	17	5

S0013-4651(99)02-078-9 CCC: $7.00 © The Electrochemical Society, Inc.

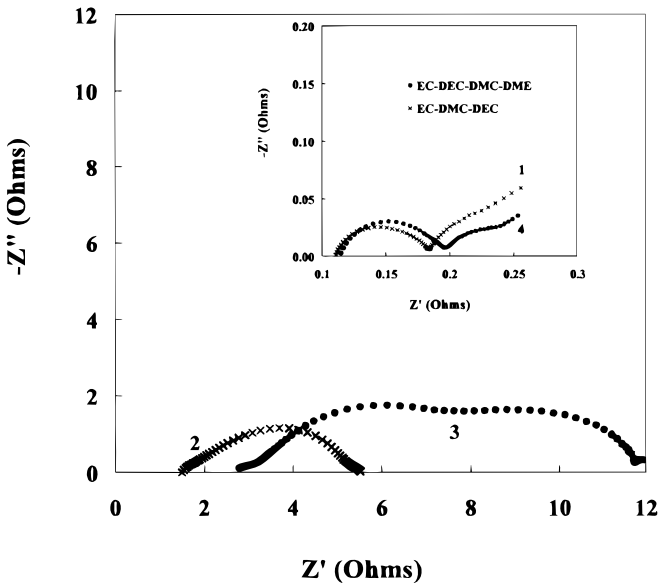

Figure 3. Nyquist plots of graphite anode in electrolytes containing 0.75 M $LiPF_6$ and different solvent mixtures, *i.e.*, (1) EC + DEC + DMC, (2) EC + DEC + DMC + MA, (3) EC + DEC + DMC + EA, and 4) EC + DMC + DEC + DME, after about 40 cycles related to performance characterization.

also increases sharply with the ester additives in the course of cycling as a result of their reaction products contributing to enhanced cell resistance.

^{7}Li NMR analysis.—Wide-line (static) ^{7}Li NMR spectra for the six intercalated graphite samples are displayed in Fig. 4. These spectra are characterized mainly by a central transition flanked by two satellite transitions corresponding to the nuclear quadruple-split levels of a spin 3/2 nucleus (^{7}Li) residing in an axially symmetric electric field gradient.[3] The central transition is centered approximately 47 ppm from the nonintercalated reference, indicating a strong Knight shift associated with the metallic intercalated graphite compound LiC_6.[3] In addition to the main "signature" of LiC_6, there is an NMR signal intensity which varies among the samples centered around zero ppm. The spectral components near zero ppm are attributed to nonintercalated Li species residing in the SEI. However, the possibility of detecting such a signal due to the presence of electrolyte species either trapped in the grain boundaries, cointercalated, or residual electrolyte from incomplete washing cannot be ruled out. Detection and characterization of these nonintercalated species by NMR has been reported previously in graphite[3] and disordered carbon.[4-6]

In addition to the intercalated and nonintercalated Li, the electrode cycled in the ternary electrolyte displays a small feature at about 260 ppm which is attributed to metallic Li,[7] accounting for ~3% of the total Li in the sample. The presence of metallic lithium in the graphite anode was later confirmed by TEM measurement. A closer look at the voltage profile during the last lithiation before cell disassembly revealed that the potential of the graphite anode momentarily spiked to negative values (*vs*. Li) before reversing to positive values. However, it is unclear why such overshoots in potential were observed, even though the film resistance in the ternary system is not high compared to carbon in other electrolytes. The graphite electrode cycled in the DME-based solution exhibited an unusually large nonintercalated feature arising from approximately half the total lithium in the sample, which is in good agreement with its large irreversible electrochemical capacity.

To better resolve the distinct spectral components corresponding to intercalated and nonintercalated lithium, high-resolution spectra were obtained by spinning about 1° off the magic angle (to reduce the side band intensity), as shown in Fig. 5. Under these conditions, the intercalated and nonintercalated lithium can be distinguished more clearly. The amount of Li associated with each of these spectral components can be determined by direct integration of the corresponding peak intensities. This procedure has been performed for both the wide-line and high-resolution spectra shown in Fig. 4 and 5, respectively. Before integration, however, one must be confident of the correct assignment of intensities to each component. This can

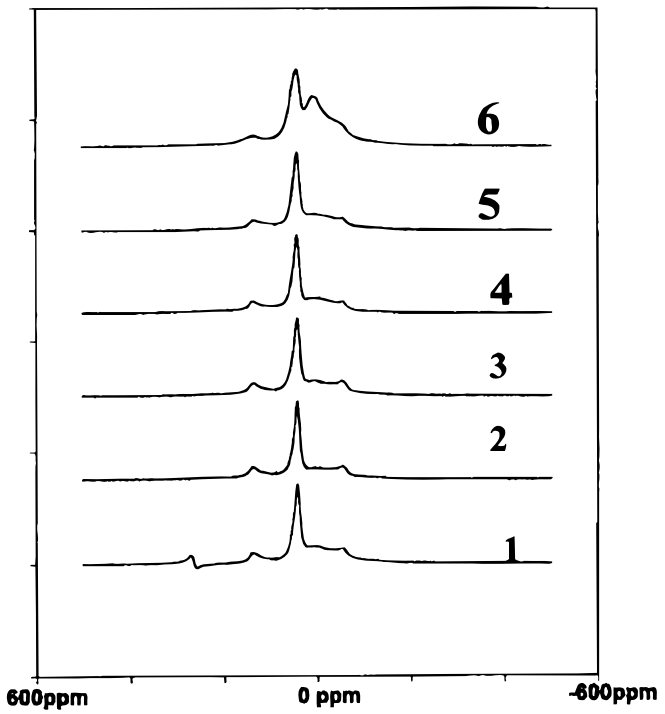

Figure 4. Wide-line ^{7}Li NMR spectra of (lithiated) cycled graphite electrodes in contact with electrolytes containing solvent mixtures of (1) EC + DEC + DMC, (2) EC + DMC, (3) EC + DEC, (4) EC + DEC + DMC + MA, (5) EC + DEC + DMC + EA, and (6) EC + DMC + DEC + DME.

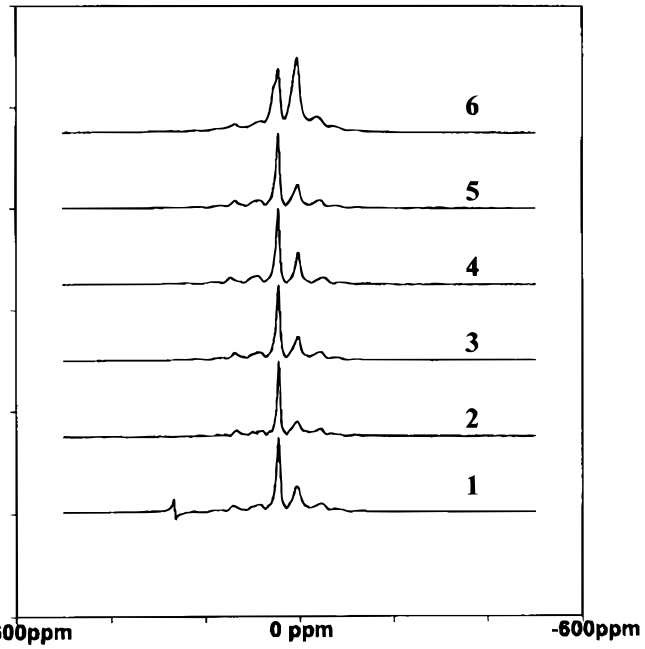

Figure 5. High-resolution ^{7}Li NMR spectra of (lithiated) cycled graphite electrodes as in Fig. 4.

S0013-4651(99)02-078-9 CCC: $7.00 © The Electrochemical Society, Inc.

be complicated by substantial overlap in the case of the wide-line spectra, which also contains significant intensity from the satellite transitions, and inclusion of side-band intensity in the high-resolution case. Thus, both sets of spectra were simulated to assist in intensity assignment. Figure 6 displays the (a) wide-line and (b) high-resolution results for graphite in the ternary system where the metallic Li component was omitted (the integrated intensity of the metallic Li is added in later). A similar procedure was performed for the electrode in the DMC-based solution, the results of which are shown in Fig. 7, (a) wide line and (b) high resolution. Before discussing these results further, an important and unanticipated result observed in both these cases, under both wide-line and high-resolution conditions, is that the central peak associated with intercalated lithium cannot be fitted with a single resonance. In the simulations presented in Fig. 6 and 7, two overlapping Knight-shifted peaks were required to replicate the experimental signal corresponding to intercalated graphite. One peak is centered at 47 ppm whereas the second, considerably smaller peak is centered at 52 ppm. That the best fit of the experimental line asymmetry is with two inequivalent Knight shifts of values cited previously is strongly justified by the fitting procedure having been applied to both the low-resolution (Fig. 6a and 7a) and high-resolution (Fig. 6b and 7b) spectra, both sets giving essentially the same result. Recent NMR results on electrochemically intercalated graphite have also suggested the presence of more than one overlapping intercalated lithium phase, for example, LiC_6 and LiC_{12}, which are characterized by Knight shifts which differ by less than 10 ppm. Additional evidence for more than one intercalated Li phase is presented later in the results from XRD and TEM experiments.

Comparison of the nonintercalated Li from NMR and EIS.—For the purpose of isolating the NMR intensity associated with the nonintercalated Li, no distinction is made between intercalated species (at 47 and 52 ppm) in the total integrated intensities. From the wide-line simulations, the intensities corresponding to nonintercalated Li for each sample are included in Table I (the MAS simulation results were similar). When the intensities corresponding to nonintercalated Li from NMR are compared with the irreversible capacities (after the fifth cycle) in Table I, it is clear the all-carbonate electrolytes have similar NMR intensities as well as irreversible capacities. Also, in the DME-based solution, the intensity corresponding to nonintercalated Li is the highest, which is also consistent with its high irreversible capacity. In the solutions with ester additives, on the other hand, the intensities corresponding to nonintercalated Li from the NMR are relatively high compared to what might be expected from their (low) irreversible capacities. This may be because the irreversible capacities in Table I are the cumulative values over the first five charge-discharge cycles in which the SEI was formed, whereas the intensities corresponding to nonintercalated Li are the values after about 40 cycles. During these cycles, there would be continued reaction between the anode and electrolyte, leading to a buildup of the SEI. The ester additives were indeed observed to show such continued reaction with the anode, as evident from a progressive decay

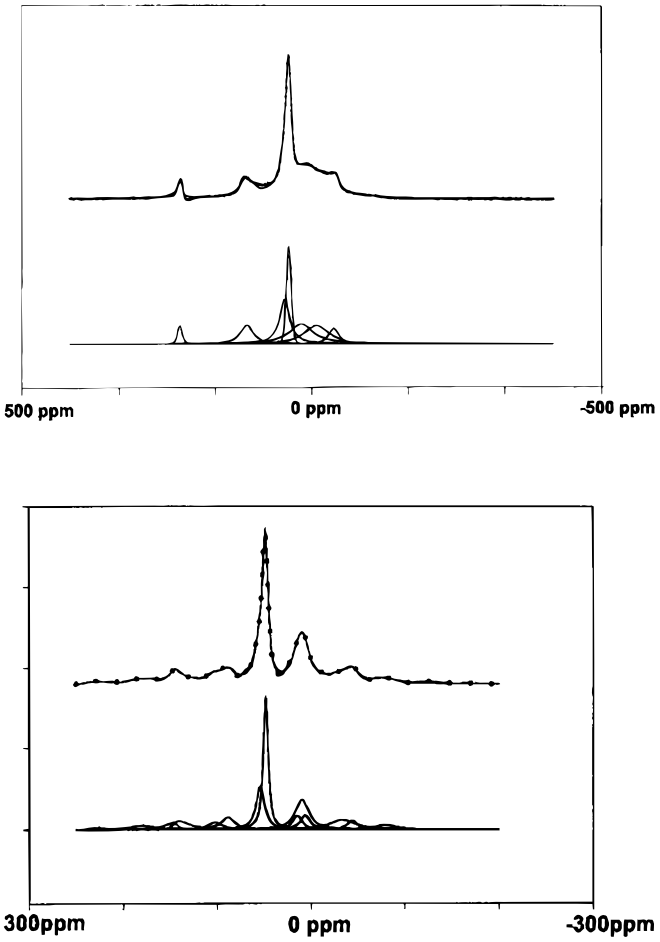

Figure 6. (a, top) Wide-line and (b, bottom) high-resolution ^{7}Li NMR spectra of (lithiated) cycled graphite electrodes in contact with electrolytes containing EC + DEC + DMC. The experimental data (points) are superimposed on simulated spectrum (solid curve). The bottom figure shows the spectral components used in the simulations.

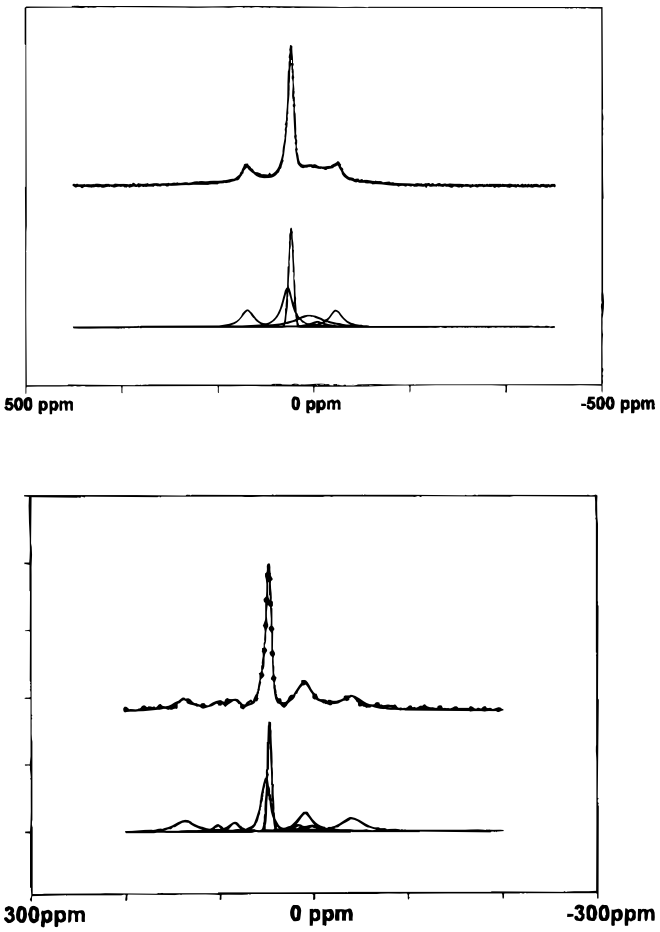

Figure 7. (a, top) Wide-line and (b, bottom) high-resolution ^{7}Li NMR spectra of (lithiated) cycled graphite electrodes in contact with electrolytes containing EC + DMC. The experimental data (points) are superimposed on simulated spectrum (solid curve). The bottom figure shows the spectral components used in the simulations.

S0013-4651(99)02-078-9 CCC: $7.00 © The Electrochemical Society, Inc.

in the intercalation kinetics.[5] The surface films formed in ester-based solutions may thus be viewed as thin (evident from low irreversible capacities) and resistive initially but are not protective enough to prevent their buildup during cycling. In the absence of the values for the irreversible capacities after 40 cycles, we have attempted to estimate the SEI buildup from film resistance values obtained from ac impedance measurements (Table II). Figure 8 shows the variation of the SEI resistance, NMR nonintercalated intensities, and irreversible capacities (fifth cycle) with the solvent composition. The film resistance is relatively low in the all-carbonate electrolyte solutions compared to the solutions with ester additives in which it increases during cycling. The high NMR intensities in the ester-based solutions (especially EA-based) might be understood in terms of the increased film resistance. In the DME-based solutions the film resistance is low, despite high irreversible capacity and high NMR nonintercalated intensity. This may possibly be due to increased surface area of the graphite anode in contact with this electrolyte, as evident from XRD data of the following section, which would explain both the low film resistance as well as high irreversible capacity. Alternately, we may speculate this to be due to the formation of less protective, probably porous surface films in the DME-based solutions.

X-ray diffraction.—To verify the existence of multiple staging compounds of graphite (*i.e.*, LiC_6 and LiC_{12}) suggested by the Li NMR data, XRD measurements were performed on the same samples of cycled graphite electrodes. As illustrated in Fig. 9, XRD confirms the presence of LiC_6 and LiC_{12} phases in the graphite anode materials.[21,22] Lithiated graphite ranges in color from blackish blue to a golden green, depending on the predominance of the LiC_6 (golden yellow) or LiC_{12} (blue/black).[20] The anode materials tested here displayed colors associated with the LiC_6 and LiC_{12} phases to varying degrees. Though all the graphite anodes were charged to a potential of 25 mV *vs.* Li, the true potential imposed on the electrodes could differ depending on the resistance of the SEI, which in turn could result in different concentrations of LiC_6 and LiC_{12}. We believe LiC_6 and LiC_{12} are the two Li environments observed by NMR.

Compared to the anodes in the other five solutions, the XRD peaks are relatively broad for the electrode cycled in the DME-containing solutions (curve 6 in Fig. 9). X-ray line broadening of this sort is indicative of strains or smaller crystallite sizes in the material. Although the electrode materials were all the same initially, lithiation-delithiation in the DME-based solution has distorted the carbon crystallites. This may possibly be due to a partial cointercalation of the solvent species (DME) into the graphite. The resultant increase in the anode surface area in this solution may be partly

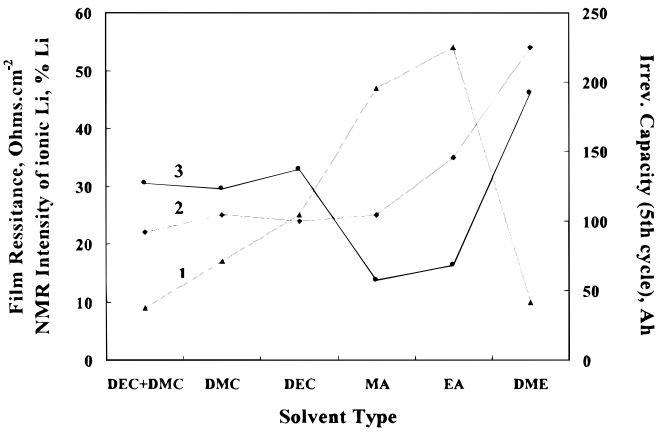

Figure 8. Variation of (1) SEI resistance from ac impedance and (2) nonintercalated intensity from ^{7}Li NMR and (3) irreversible capacities of graphite electrodes in contact with electrolytes containing different solvent mixtures, *i.e.*, EC + DEC + DMC, EC + DMC, EC + DEC, EC + DEC + DMC + MA, EC + DEC + DMC + EA, and EC + DMC + DEC + DME.

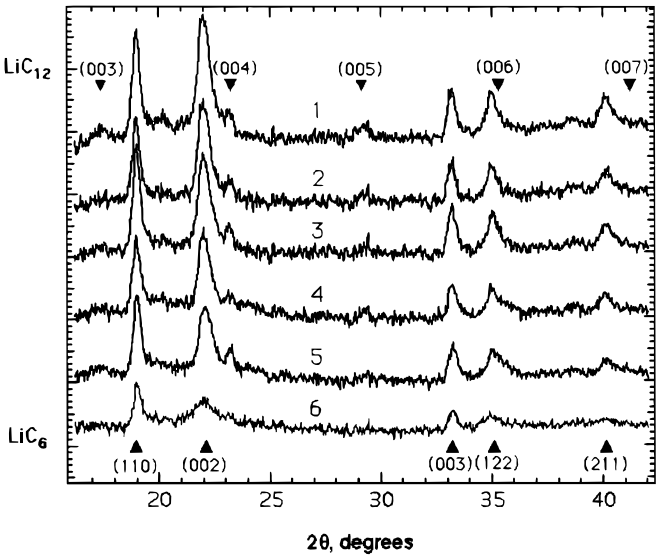

Figure 9. XRD patterns of (lithiated) cycled graphite electrodes in contact with electrolytes containing solvent mixtures of (1) EC + DEC + DMC, (2) EC + DMC, (3) EC + DEC, (4) EC + DEC + DMC + MA, (5) EC + DEC + DMC + EA, and (6) EC + DMC + DEC + DME.

responsible for the observed high irreversible capacity and low film (SEI) resistance from EIS measurements.

Measuring the areas under the 005 peak of the LiC_{12} phase and 003 peak of the LiC_6 phase, we were able to estimate relative phase fractions present in the graphite anode materials. Approximately, the phase fractions reveal 80-95% of reversible Li is in the LiC_6 phase, with the bulk of the remainder in LiC_{12} phase. These numbers are not precise because the XRD patterns were acquired from small samples of heterogeneous material.

Transmission electron microscopy.—The transmission electron micrographs show a heterogeneous distribution of phases in the graphite samples. The microstructure of the cycled materials ranged from sheet-like graphite regions to dense polycrystals. As measured from dark-field and bright-field images (Fig. 10), the sheet-like regions were on the order of 100 nm. Moiré fringes were found in some of these regions, indicating random orientation of overlapping graphite regimes. The crystallites in the polycrystalline regions were very small and of the order of 10 nm. These polycrystalline regions could be areas of low-strain, organized carbon surrounded by highly buckled or tetrahedrally bonded carbon.[21]

Electron energy loss spectrometry.—EELS was used to determine the presence of intercalated and metallic Li. Intercalated Li

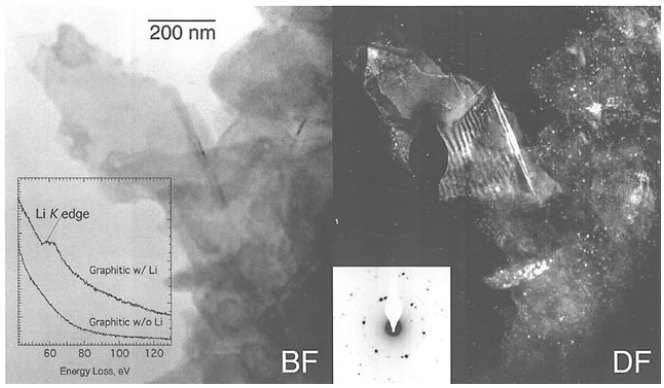

Figure 10. Dark-field and bright-field TEMs and EELS of cycled graphite electrodes in contact with electrolytes containing solvent mixtures of EC + DMC.

S0013-4651(99)02-078-9 CCC: $7.00 © The Electrochemical Society, Inc.

was observed in both polycrystalline and sheet-like regions. Figure 10 shows spectra for both polycrystalline and sheet like regions. The characteristic Li K-edge at 52 eV is seen in both the sheet-like and polycrystalline regions, although regions showing similar morphology and thickness were found to be without Li. Plasmons for metallic Li were observed on graphite electrodes in the electrolyte containing the ternary solvent mixture (solution number 1). This observation of metallic lithium was consistent with the results from the ^{7}Li NMR spectra.

Conclusions

Various solvent mixtures are being studied to improve the low-temperature performance of lithium-ion cells. These solvent mixtures use alkyl carbonate mixtures that have favorable filming properties, with quaternary additives of low viscosity and melting point, such as MA, EA, and DME. The characteristics of the surface films (SEI) on graphite are observed to be strongly affected by the solvent additives. The irreversible and reversible capacities are also influenced strongly by the electrolyte composition. Quantitative determination of irreversible Li content was obtained by integrating the ^{7}Li NMR spectral components associated with the Knight-shifted intercalated Li and unshifted Li species residing in the SEI. The NMR results were in qualitative agreement with the electrochemical determinations. From a combination of EIS, charge-discharge behavior, and ^{7}Li NMR data, it may be postulated that compact, barrier-type, protective films are formed in solutions based on alkyl carbonate, whereas bulky, porous, and less protective films are formed with DME additives. X-ray diffractometry indicated that the DME-additive caused microstructural damage to the graphite, perhaps by cointercalation. Ester additives result in surface films that are compact but resistive initially and were observed to grow considerably during cycling. The presence of at least two distinct intercalated Li phases (LiC_{12} and LiC_6) in the graphite electrodes were observed by NMR and XRD. In addition, metallic Li was also observed in one sample from the NMR and TEM data.

Acknowledgments

The work described here was carried out at the Jet Propulsion Laboratory, California Institute of Technology, under contract with the National Aeronautics and Space Administration and was supported by the Mars Exploration Program, NASA Code S Battery program, and a DARPA-sponsored TRP program. The TEM studies and the Li NMR studies were carried at the California Institute of Technology and Hunter College, respectively, and were supported by grants from the Department of Energy (Office of Basic Energy Sciences, DE-FG03-94ER14493) and the Office of Naval Research. One of the authors (S.G.G.) acknowledges the National Research Council for Fellowship support during his sabbatical leave at the Jet Propulsion Laboratory.

The Jet Propulsion Laboratory, California Institute of Technology, assisted in meeting the publication costs of this article.

References

1. O. Chusid, Y. Ein-Eli, M. Babai, Y. Carmeli, and D. Aurbach, *J. Power Sources*, **43-44,** 47 (1994); D. Aurbach, Y. Ein-Eli, O. Chusid, M. Babai, Y. Carmeli, and H. Yamin, *J. Electrochem. Soc.*, **141,** 603 (1994); D. Aurbach, Y. Ein-Eli, and B. Markovsky, *Electrochim. Acta.*, **39,** 2559 (1994); D. Aurbach, Y. Ein-Eli, B. Markovsky, A. Zabon, S. Luski, Y. Carmeli, and H. Yamin, *J. Electrochem. Soc.*, **142,** 2882 (1995).
2. E. Peled, in *Lithium Batteries*, J. P. Gabano, Editor, Chap. 3, Academic Press, New York (1983).
3. N. Imanshi, K. Kumai, H. Kokugan, Y. Takeda, and O. Yamamoto, *Solid State Ionics*, **107,** 135 (1998).
4. N. Takami, A. Satoh, T. Ohsaki, and M. Kanda, *Electrochim. Acta*, **42,** 2537 (1997).
5. Y. Dai, Y. Wang, V. Eshkenazi, E. Peled, and S. G. Greenbaum, *J. Electrochem. Soc.*, **145,** 1179 (1998).
6. M. Carewska, S. Scaccia, F. Croce, S. Arumugam, Y. Wang, and S. Greenbaum, *Solid State Ionics*, **93,** 227 (1997).
7. K. R. Morgan, S. Collier, G. Burns, and K. Ooi, *J. Chem. Soc., Chem. Commun.*, 1719 (1994).
8. C. Marichal, J. Hirshinger, P. Granger, M. Menetrier, A. Rougier, and C. Delmas, *Inorg. Chem.*, **34,** 1773 (1995).
9. M. C. Smart, C. K. Huang, B. V. Ratnakumar, and S. Surampudi, in *Proceedings of the 37th Power Sources Conference*, pp. 239-242, Cherry Hill, NJ, June 17-20, 1996; M. C. Smart, C.-K. Huang, B. V. Ratnakumar, and S. Surampudi, in *Proceedings of the 32nd IECEC*, Honolulu, HI, July 1997; M. C. Smart, B. V. Ratnakumar, C.-K. Huang, and S. Surampudi, in *Proceedings of the SAE Aerospace Power Systems Conference*, 322, pp. 7-14 (1998).
10. S. T. Meyer, H. C. Yoon, C. Bragg, and J. H. Lee, in *Proceedings of the 13th International Primary and Secondary Battery Technology and Applied Semiconductors*, Boca Raton, FL, March 1996; M. W. Juzkow, in *Proceedings of the 14th International Primary and Secondary Battery Technology and Applied Semiconductors*, Boca Raton, FL, March 1997.
11. R. Gitzendanner, G. Erlich, C. Marsh, and R. Marsh, Abstract 157, The Electrochemical Society Meeting Abstracts, Vol. 98-2, Boston, MA, Nov 1-6, 1998.
12. G. Bruce, A. Schumacher, and L. Marcoux, in *Proceedings of the 38th Power Sources Conference*, p. 444, Cherry Hill, NJ, June 8-11, 1998; L. Marcoux, in *SAE Conference 98*, Williamsburg, VA, Aug 1998; G. Bruce, P. Mardikian, and L. Marcoux, in *Proceedings of the 33rd IECEC*, Colorado Springs, CO, Aug 1998.
13. E. J. Plicta and W. K. Behl, in *Proceedings of the 38th Power Sources Conference*, p. 444, Cherry Hill, NJ, June 8-11, 1998.
14. (a) Y. Ein-Eli, S. R. Thomas, R. Chadha, T. J. Blakley, and V. R. Koch, *J. Electrochem. Soc.*, **144,** 823 (1997); (b) Y. Ein-Eli, S. R. Thomas, and V. R. Koch, *J. Electrochem. Soc.*, **143,** L195 (1996); (c) Y. Ein-Eli, S. R. Thomas, and V. R. Koch, *J. Electrochem. Soc.*, **144,** 1159 (1997); (d) Y. Ein-Eli, S. R. Thomas, R. Chadha, T. J. Blakley, and V. R. Koch, *J. Electrochem. Soc.*, **143,** 823 (1996); (e) Y. Ein-Eli, S. R. Thomas, V. R. Koch, D. Aurbach, B. Markovsky, and Schechter, *J. Electrochem. Soc.*, **143,** L273 (1996); (f) Y. Ein-Eli, S. F. McDevitt, D. Aurbach, B. Markovsky, and A. Schechter, *J. Electrochem. Soc.*, **144,** L180 (1997).
15. M. C. Smart, B. V. Ratnakumar, and S. Surampudi, *J. Electrochem. Soc.*, **146,** 486 (1999).
16. A. H. Ohta, H. Koshina, H. Okuno, and H. Murai, *J. Power Sources*, **54,** 6 (1995).
17. D. Aurbach and E. Granot, *Electrochim. Acta.*, **42/44,** 697 (1997).
18. M. Wagner, *Electrochim. Acta*, **42,** 1623 (1997).
19. B. A. Boukamp, *Solid State Ionics*, **20,** 31 (1986).
20. S. Basu, G. K. Wertheim, and S. B. Dicenzo, in *Lithium: Current Applications in Science, Medicine, and Technology*, R. O. Bach, Editor, John Wiley & Sons, New York (1985).
21. J. R. Dahn, *Phys. Rev. B*, **44,** 9170 (1991).
22. M. Morita, T. Ichimura, M. Ishikawa, and Y. Matsuda, *J. Electrochem. Soc.*, **143,** L26 (1996).
23. J. R. Dahn, A. K. Sleigh, H. Shi, B. M. Way, W. J. Weydanz, J. N. Reimers, Q. Zhong, and U. von Sacken, in *Lithium Batteries*, G. Pistoia, Editor, Chap. 1, Elsevier, London (1994).